Available online at www.sciencedirect.com
SCIENCE DIRECT®
Journal of Sound and Vibration 277 (2004) 971–986
JOURNAL OF SOUND AND VIBRATION
www.elsevier.com/locate/jsvi

Identification of complex moduli and Poisson's ratio from measured strains on an impacted bar

S. Mousavi, D.F. Nicolas, B. Lundberg*

The Ångström Laboratory, Uppsala University, Box 534, SE-751 21 Uppsala, Sweden

Received 21 May 2003; accepted 22 September 2003

Abstract

The complex extension modulus, the complex shear modulus and the complex Poisson's ratio at room temperature have been identified from strain measurements on test bars made of polymethyl methacrylate (PMMA) and polypropylene (PP) which were subjected to axial and torsional impacts. Bars of each material with diameters 10 and 20 mm were tested at low and high levels of excitation for each mode of impact. The complex moduli were identified from the normal and shear strain histories at five non-uniformly distributed bar sections, while the complex Poisson's ratio was determined from the circumferential and axial normal strain histories at a single bar section. With the 10 mm test bars, satisfactory results were obtained from about 1 to 40 kHz for PMMA and from about 1 to 15 kHz for PP. Under the conditions of the tests, the responses of both materials were found to be very close to linear and nearly isotropic. The deviation from isotropy was larger for PP than that for PMMA, especially for the 10 mm test bars. A certain influence of the test bar dimension on the complex moduli was observed, especially for PP at low frequencies. The influence of test bar dimension on the observed deviation from isotropy and on the complex moduli for PP is believed to be partly due to the extrusion and cooling processes used for fabrication of the PP test bars.

1. Introduction

The ability to assess whether the response of a viscoelastic material to a mechanical load is linear or non-linear and whether it is isotropic or anisotropic is a prerequisite for the use of such materials in engineering. If a viscoelastic material has a linear response, its constitutive

*Corresponding author. Tel.: +46-18-4713125; fax: +46-18-471-3122.
E-mail address: bengt.lundberg@angstrom.uu.se (B. Lundberg).

0022-460X/$ - see front matter © 2003 Elsevier Ltd. All rights reserved.
doi:10.1016/j.jsv.2003.09.053

properties can be represented by two or more complex-valued functions of angular frequency ω. If the response is also isotropic, the number of independent such constitutive functions is minimal. Examples of constitutive functions in common use for isotropic materials are the complex extension modulus $E(\omega)$, the complex shear modulus $G(\omega)$ and the complex Poisson's ratio $v(\omega)$, which are interrelated by $G = E/2(1 + v)$. The relative magnitudes of the complex moduli for a given material has been considered by Theocaris [1], while the general frequency dependencies of these moduli and of the complex Poisson's ratio have been examined by Pritz [2].

Methods for identification of constitutive functions at relevant frequencies and temperatures have important uses in engineering. For components and structures which are loaded dynamically, frequencies of interest may typically vary from hundreds of Hz to tens of kHz. In this frequency range, use can be made of identification methods based on wave propagation in a test specimen. Several such methods for identification of the complex extension modulus [3–18], the complex shear modulus [19] and the complex Poisson's ratio [20] have been developed.

Methods based on measurement of waves which do not overlap at instrumented sections have been employed by, for example, Refs. [3–9]. In the cases of quasi-longitudinal or torsional waves such methods require only two independent measurements, or one if a boundary condition is used, and they are mathematically simple. However, they may require relatively long test bars. Methods which permit overlap of waves at instrumented sections have been used by, for example, Refs. [10–18]. Such methods admit the use of relatively short test bars. However, they require at least three independent measurements for quasi-longitudinal or torsional waves, or two if a boundary condition is used, and they are mathematically more complex. In the case of flexural waves in beams they require at least five independent measurements, or four if a boundary condition is used [17].

The aim of this study was to develop a procedure, based on propagation of waves in a single test bar, for the identification of the complex extension modulus $E(\omega)$, the complex shear modulus $G(\omega)$ and the complex Poisson's ratio $v(\omega)$. Inherent in this procedure was the assessment of linearity, isotropy and dependence on test specimen, and the procedure was applied to two materials of importance in engineering, viz., polymethyl methacrylate (PMMA) and polypropylene (PP).

The wave propagation method employed for the complex moduli was the one used by Hillström et al. [16]. This method, originally used for identification of the complex extension modulus from analysis of quasi-longitudinal waves, was adapted to identification of the complex shear modulus from analysis of torsional waves. Normal and shear strain histories were measured at four sections of a cylindrical test bar with circular cross-section subjected to axial and torsional impact, respectively. Use was also made of the boundary conditions at the free non-impacted ends of the test bars, which means that two strain measurements were redundant. The complex Poisson's ratio was identified on the basis of measured strain histories in the circumferential and axial directions at a single section of a cylindrical test bar subjected to axial impact.

The 1D model used for the two types of waves and the identification method are presented in Section 2, and the experimental equipment and procedures are presented in Section 3. The results are presented and discussed in Section 4. Nomenclature is listed in Appendix A.

2. Theory

2.1. Quasi-longitudinal and torsional waves in a test bar

Consider propagation of quasi-longitudinal or torsional waves in a straight cylindrical test bar with circular cross-section and radius a. Let the material of the test bar be linearly viscoelastic and isotropic with density ρ, complex extension modulus $E(\omega)$, complex shear modulus $G(\omega)$ and complex Poisson's ratio $v(\omega)$, where ω is the angular frequency. Because of the assumed isotropy, the constitutive properties $E(\omega)$, $G(\omega)$ and $v(\omega)$ are interrelated through $G = E/2(1+v)$. Let r, φ, and z be cylindrical co-ordinates.

The waves considered are governed by the temporally Fourier transformed wave equation

$$\partial^2\hat{\varepsilon}/\partial z^2 - \gamma^2\hat{\varepsilon} = 0. \tag{1}$$

Here $\hat{\varepsilon}(z,\omega) = \int_{-\infty}^{\infty} \varepsilon(z,t)\mathrm{e}^{-\mathrm{i}\omega t}\,\mathrm{d}t$ is the temporal Fourier transform of the relevant surface strain, and $\gamma(\omega) = \alpha(\omega) + \mathrm{i}k(\omega)$ is a wave propagation coefficient defined by

$$\gamma^2(\omega) = -\rho\omega^2/M(\omega), \tag{2}$$

where $M(\omega)$ is the relevant complex modulus. The damping coefficient $\alpha(\omega)$ is a positive even function, and the wavenumber $k(\omega)$ is an odd function, positive for $\omega > 0$ [21].

The general solution of Eq. (1) is

$$\hat{\varepsilon}(z,\omega) = \hat{P}(\omega)\mathrm{e}^{-\gamma(\omega)z} + \hat{N}(\omega)\mathrm{e}^{\gamma(\omega)z}, \tag{3}$$

where $\hat{P}(\omega)$ and $\hat{N}(\omega)$ are complex amplitudes of harmonic waves travelling in the directions of increasing and decreasing z, respectively. For $\omega > 0$, the wavelength λ can be expressed in terms of the wavenumber k as

$$\lambda(\omega) = 2\pi/k(\omega). \tag{4}$$

In the case of quasi-longitudinal waves $\varepsilon(z,t) = \varepsilon_{zz}(a,z,t)$ and $M(\omega) = E(\omega)$, and Eq. (1) is based on the assumptions that plane cross-sections remain plane, stress is uni-axial and the effect of radial inertia can be neglected. Also, $\varepsilon_{zz}(r,z,t) = \varepsilon_{zz}(a,z,t)$, σ_{zz} is the only non-zero component of stress, and the strains ε_{zz} and $\varepsilon_{\varphi\varphi}$ are related through $\hat{\varepsilon}_{\varphi\varphi}(r,z,\omega) = -v(\omega)\hat{\varepsilon}_{zz}(r,z,\omega)$. As, in particular, this relation is valid for $r = a$, it is possible to obtain the complex Poisson's ratio directly from measured surface strains $\hat{\varepsilon}_{\varphi\varphi 0}(\omega)$ and $\hat{\varepsilon}_{zz0}(\omega)$ at $z = z_0$ as

$$v(\omega) = -\hat{\varepsilon}_{\varphi\varphi 0}(\omega)/\hat{\varepsilon}_{zz0}(\omega). \tag{5}$$

Because of the simplifying assumptions made, the results obtained from this 1D model can be expected to be accurate if and only if the wavelength is much larger than the transverse dimension of the bar, i.e.,

$$\lambda_{\mathrm{L}}(\omega) \gg a. \tag{6}$$

In the case of torsional waves, $\varepsilon(z,t) = \varepsilon_{\varphi z}(a,z,t)$ and $M(\omega) = G(\omega)$, and Eq. (1) can derived from the assumption that plane cross-sections remain plane and rigid as they rotate around the z-axis. Also, $\varepsilon_{\varphi z}(r,z,t) = (r/a)\varepsilon_{\varphi z}(a,z,t)$ is the only non-zero component of strain. Here, the assumed 1D mode of motion satisfies the 3D equations of elasticity, in the interior of the bar as

well as on its cylindrical boundary $r = a$. Therefore, there is no restriction on the wavelength $\lambda_{\leftrightarrows T}$ corresponding to Eq. (6).

2.2. Identification of complex moduli

The procedure for identification of the complex modulus M, representing E or G, is the same as that used by Hillström et al. [16] for identification of E. Thus, n surface strains $\hat{\varepsilon}_1(\omega)$, $\hat{\varepsilon}_2(\omega)$, …, $\varepsilon_n(\omega)$ at sections $z_1 < z_2 < \cdots < z_n$ are considered to be known either from measurements alone or from measurements and the boundary condition at a free bar end (where $\hat{\varepsilon}(\omega)$ is zero). This gives the system of n equations

$$\mathbf{A}(\omega)\hat{\mathbf{w}}(\omega) = \hat{\boldsymbol{\varepsilon}}(\omega), \tag{7}$$

where

$$\mathbf{A}(\omega) = \begin{bmatrix} e^{-\gamma(\omega)z_1} & e^{\gamma(\omega)z_1} \\ e^{-\gamma(\omega)z_2} & e^{\gamma(\omega)z_2} \\ \vdots & \vdots \\ e^{-\gamma(\omega)z_n} & e^{\gamma(\omega)z_n} \end{bmatrix}, \quad \hat{\mathbf{w}}(\omega) = \begin{bmatrix} \hat{P}(\omega) \\ \hat{N}(\omega) \end{bmatrix}, \quad \hat{\boldsymbol{\varepsilon}}(\omega) = \begin{bmatrix} \hat{\varepsilon}_1(\omega) \\ \hat{\varepsilon}_2(\omega) \\ \vdots \\ \hat{\varepsilon}_n(\omega) \end{bmatrix}, \tag{8}$$

and the three complex-valued functions $\gamma(\omega)$, $P(\omega)$ and $N(\omega)$ are unknown. If system (7) can be solved for $\gamma(\omega)$, the complex modulus $M(\omega)$ can be obtained from Eq. (2).

If $n = 3$, there generally exists an exact solution for $\gamma(\omega)$ which corresponds to the requirements on $\alpha(\omega)$ and $k(\omega)$. At certain frequencies, however, there may not exist a solution. If $n > 3$, system (7) is over-determined, and generally there is no exact solution for $\gamma(\omega)$. In this case, however, it is generally possible to find a best approximate solution in the sense of least squares. This solution is obtained by minimizing the error

$$\tilde{e}(\hat{\mathbf{w}}, \gamma) = ||\mathbf{A}\hat{\mathbf{w}} - \hat{\boldsymbol{\varepsilon}}||/||\hat{\boldsymbol{\varepsilon}}||, \tag{9}$$

where double bars denote Euclidian norm, with respect to $\hat{\mathbf{w}}$ and γ. Here, the minimization is carried out in two steps as follows. First, $\tilde{e}(\hat{\mathbf{w}}, \gamma)$ is minimized with respect to $\hat{\mathbf{w}}$ for a given γ by letting

$$\hat{\mathbf{w}} = \hat{\mathbf{w}}_{\mathrm{LS}}(\gamma) = \mathbf{A}^{+}\hat{\boldsymbol{\varepsilon}}, \tag{10}$$

where $\mathbf{A}^{+} = (\mathbf{A}^{*}\mathbf{A})^{-1}\mathbf{A}^{*}$ is the Moore–Penrose pseudo-inverse matrix of $\mathbf{A}$, and $\mathbf{A}^{*}$ is the adjoint (complex conjugate and transpose) matrix of $\mathbf{A}$. Then, in the second step, $\tilde{e}(\hat{\mathbf{w}}_{\mathrm{LS}}(\gamma), \gamma)$ is minimized numerically with respect to γ.

3. Experiments

3.1. Test bars and instrumentation

Two different test bars with nominally circular cross-section of each of two different materials were used to identify the complex extension modulus $E(\omega)$ and the complex Poisson's ratio $\nu(\omega)$ from quasi-longitudinal wave tests and the complex shear modulus $G(\omega)$ from torsional wave

tests. The two materials used were polymethyl methacrylate (PMMA) and polypropylene (PP), and for each of them one test bar had diameter 10 mm and approximate length 1000 mm and the other had diameter 20 mm and approximate length 2000 mm.

PMMA is an amorphous thermoplastic with density 1183 kg/m^3, and PP is a semi-crystalline thermoplastic with density 915 kg/m^3. The test bars made of PMMA had been produced from moulded plates which had been cut into bars with rectangular cross-sections and then machined to obtain their final shape and dimensions. The test bars made of PP had been extruded from the melted raw material into their approximate final shape and dimensions. As they had been cooled in air on a flat surface, their cross-sections were slightly elliptical (with axis ratio $\approx$ 1.05).

Each test bar was instrumented at four different sections ($z = z_2$ to z_5) with strain gauges for measurement of the normal strains ε_{zz} and the shear strains $\varepsilon_{\varphi z}$. Use was also made of the circumstance that at a free end ($z = z_1$) of a bar these strains are zero, which provided $n = 5$ strains, two of which were redundant, for the identification of the complex extension modulus $E(\omega)$ and the complex shear modulus $G(\omega)$, respectively. In addition, each bar was instrumented at a fifth section ($z = z_0$) with strain gauges for measurement of the normal strains ε_{zz} and $\varepsilon_{\varphi\varphi}$ needed for the identification of the complex Poisson's ratio $\nu(\omega)$. The strain gauges were glued with cyanocrylate bond. The strain gauge configurations and the types of strain gauges used for the three kinds of strain measurements and the two test bar sizes are presented in Table 1.

For each strain to be measured, two diametrically opposite strain gauges were used and connected to a bridge amplifier (Measurement Group 2210) in such a way that they assisted each other in the production of output signals. As a consequence, the output signal representing the axial strain ε_{zz} became insensitive to bending which might arise due to slight eccentricity or some other imperfection. The bridge amplifiers were followed by aliasing filters (DIFA Measuring Systems, PDF), and the filtered signals were recorded by means of a four-channel digital oscilloscope (Nicolet Pro 20). The cut-off frequency and the sampling interval, respectively, were chosen differently in different tests. The recorded signals were transferred to a PC computer for processing. Shunt calibration was used.

3.2. Quasi-longitudinal wave tests

The experimental set-up for identification of the complex extension modulus $E(\omega)$ is shown in Fig. 1. The test bars were suspended horizontally by thin wires and impacted axially on a flat end

Table 1
Strain gauge types and configurations

Strain gauge configuration	Measured strain	Strain gauge type	Distances of strain gauges from free end (mm)			
E10	ε_{zz}	TML GFRA-3-50-1L	145	323	539	800
G10	$\varepsilon_{z\varphi}$	TML GFRA-3-50-1L	147.5	325.5	541.5	802.5
N10	$\varepsilon_{zz},\varepsilon_{\varphi\varphi}$	TML FCB-2-23-1L	840			
E20	ε_{zz}	TML GFLA-6-350-70	280	636	1068	1590
G20	$\varepsilon_{z\varphi}$	TML QFCT-2-350-11-6F-1L	280	636	1068	1590
N20	$\varepsilon_{zz},\varepsilon_{\varphi\varphi}$	TML GFLA-6-350-70	986			

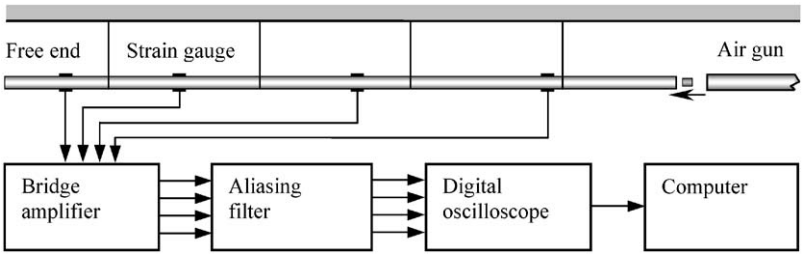

Fig. 1. Experimental set-up for identification of the complex extension modulus E and the complex Poisson's ratio v on the basis of quasi-longitudinal wave propagation tests with 10 and 20 mm test bars.

by projectiles fired from an air gun. For the 10 mm test bars, use was made of lead bullets with mass 0.54 g and approximate impact velocities 60 and 90 m/s at low and high levels of excitation, respectively. For the 20 mm test bars, the projectiles used had diameter 8 mm and length 10 mm, were made of the same material as the test bars, and had approximate impact velocities 90–140 and 200–500 m/s at low and high levels of excitation, respectively. The non-impacted end of each test bar ($z = z_1$) was kept free. One normal strain ε_{zz} was measured at each of four sections ($z = z_2$ to z_5). The conditions for eight tests (1–8) carried out with the two materials, the two bar diameters and the two excitation levels are defined in Table 2.

The experimental set-up for identification of the complex Poisson's ratio $v(\omega)$ was similar but only two normal strains ε_{zz} and $\varepsilon_{\varphi\varphi}$ at a single section ($z = z_0$) associated with the passage of the incident pulse were measured. The conditions for four tests (9–12) carried out with the two materials and the two bar diameters are defined in Table 2.

3.3. Torsional wave tests

The experimental set-up for identification of the complex shear modulus $G(\omega)$ is shown in Fig. 2. The 10 mm test bars were suspended horizontally by thin wires and by a slide bearing at the impacted end. Immediately outside the bearing, the originally flat end of each test bar had been modified by removing a 90° sector over a length of 7 mm. One of the flat surfaces of the resulting open sector was impacted in the normal direction (i.e., transversely to the bar axis) by a projectile fired from an air gun so that the bar end was subjected to combined torsion and bending. Because of the bearing, however, the instrumented part of the test bar was subjected to torsion but prevented from bending. The 20 mm test bars were kept in vertical position by slide bearings at each end. Torsion in the instrumented parts of the test bars was generated similar to that in the 10 mm bars. However, a high-strength aluminium ring with a flat surface was clamped on the impacted end instead of removing a 90° sector. For the 10 mm test bars, use was made of lead bullets with mass 0.54 g and approximate impact velocities 60 and 90 m/s at low and high levels of excitation, respectively. For the 20 mm test bars, the projectiles used had diameter 8 mm and length 10 mm, were made of the same material as the test bars, and had approximate impact velocities 90–140 and 200–500 m/s at low and high levels of excitation, respectively. The non-impacted end of each test bar ($z = z_1$) was kept free. One shear strain $\varepsilon_{\varphi z}$ was measured at each of

Table 2
Test conditions

Test	Quantity	Material	Diameter (mm)	Excitation	Strain gauges	Cut-off freq. (kHz)	Sampling freq. (kHz)	Max strain ($\times 10^{-3}$)	Temp. (°C)
1	E	PMMA	10	High	E10	100	500	3.8	20.5
2	E	PMMA	10	Low	E10	100	500	2.0	20.5
3	E	PMMA	20	High	E20	35	100	2.4	21.0
4	E	PMMA	20	Low	E20	35	100	1.1	21.0
5	E	PP	10	High	E10	100	500	2.8	21.5
6	E	PP	10	Low	E10	100	500	0.15	21.5
7	E	PP	20	High	E20	35	100	1.2	21.2
8	E	PP	20	Low	E20	35	100	0.36	21.2
9	ν	PMMA	10	–	N10	100	500	2.4	22.4
10	ν	PMMA	20	–	N20	35	100	2.1	22.0
11	ν	PP	10	–	N10	100	500	2.3	22.6
12	ν	PP	20	–	N20	35	100	0.39	21.5
13	G	PMMA	10	High	G10	100	500	5.2	22.0
14	G	PMMA	10	Low	G10	100	500	2.7	22.0
15	G	PMMA	20	High	G20	20	100	3.3	21.0
16	G	PMMA	20	Low	G20	35	100	0.94	22.0
17	G	PP	10	High	G10	100	500	5.1	21.7
18	G	PP	10	Low	G10	100	500	3.0	21.7
19	G	PP	20	High	G20	35	100	1.4	21.9
20	G	PP	20	Low	G20	35	100	0.47	21.9

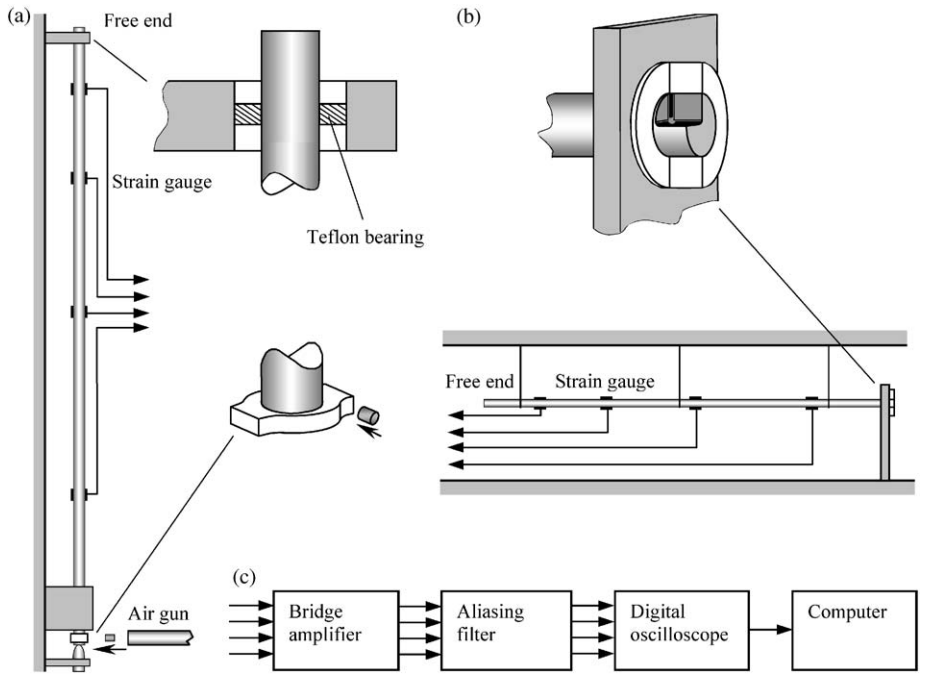

Fig. 2. Experimental set-up for identification of the complex shear modulus G on the basis of torsional wave propagation tests with horizontal 10 mm and vertical 20 mm test bar.

four sections ($z = z_2$ to z_5). The conditions for eight tests (13–20) carried out with the two materials, the two bar diameters and the two excitation levels are defined in Table 2.

4. Results and discussion

The wavelength λ, the complex extension modulus E, the complex shear modulus G, the complex Poisson's ratio v and related quantities for PMMA and PP, obtained experimentally at room temperature with 10 and 20 mm test bars at high and low levels of impact excitation, are shown versus frequency $f = \omega/2\pi$ in Figs. 3–13. Each result for λ, E, G and v is based on a single test, and only Figs. 9 and 10 contain results which are based on tests with low-level impact excitation.

The dispersion relationships for quasi-longitudinal and torsional waves in the test bars, expressed as wavelength λ versus frequency f, are shown in Fig. 3 for PMMA and in Fig. 4 for PP. For PMMA, the wavelength of quasi-longitudinal waves is approximately 55 mm or $11a$ at 40 kHz for the 10 mm test bar and 150 mm or $15a$ at 15 kHz for the 20 mm test bar. For PP, the wavelength of quasi-longitudinal waves is approximately 120 mm or $24a$ at 15 kHz for the 10 mm test bar and 150 mm or $15a$ at 12 kHz for the 20 mm test bar. Because of condition (6) and convergence problems above certain frequencies for PP, results are shown for PMMA up to 40 and 15 kHz for the 10 and 20 mm test bars, respectively, and for PP up to 15 kHz for both test bars.

The complex moduli E and G, and the complex Poisson's ratio v, are shown versus frequency f in Fig. 5 for PMMA and in Fig. 6 for PP. For PMMA the real parts of E and G increase at low frequencies and are nearly constant at higher frequencies. The imaginary parts appear to have maxima at low frequencies and are nearly constant at higher frequencies. For PP the behaviour of the real parts of E and G are similar to those of PMMA, while the imaginary parts increase at low frequencies and are nearly constant at higher frequencies. For both PMMA and PP v is, apart from the noise, approximately real and constant throughout the frequency ranges studied.

The loss angles $\delta_E = \arg(E)$ and $\delta_G = \arg(G)$ associated with the complex moduli are shown versus frequency f in Fig. 7 for PMMA and in Fig. 8 for PP. For PMMA these loss angles have

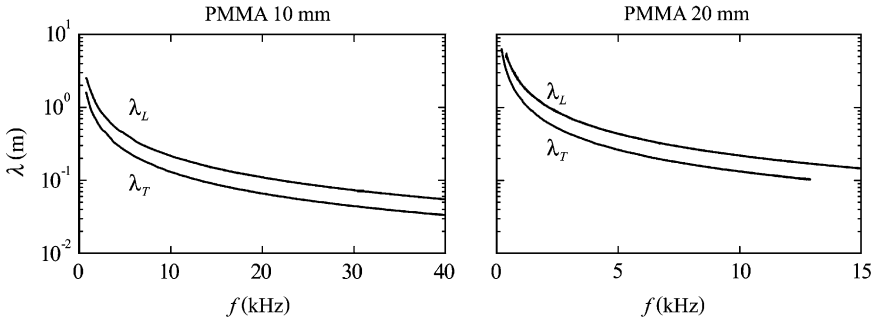

Fig. 3. Wavelength λ versus frequency f for quasi-longitudinal (index L) and torsional (index T) waves in 10 and 20 mm PMMA test bars.

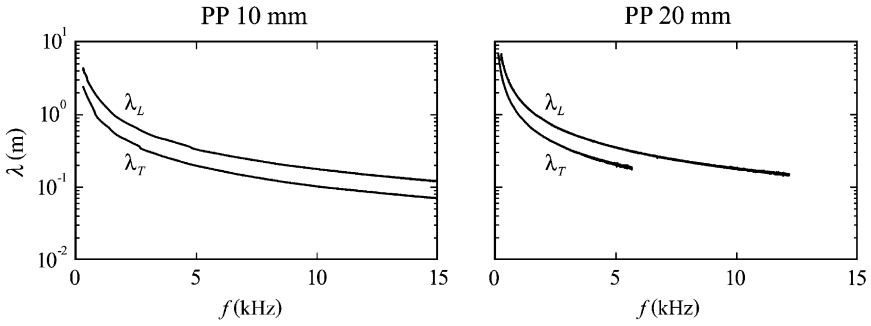

Fig. 4. Wavelength λ versus frequency f for quasi-longitudinal (index L) and torsional (index T) waves in 10 and 20 mm PP test bars.

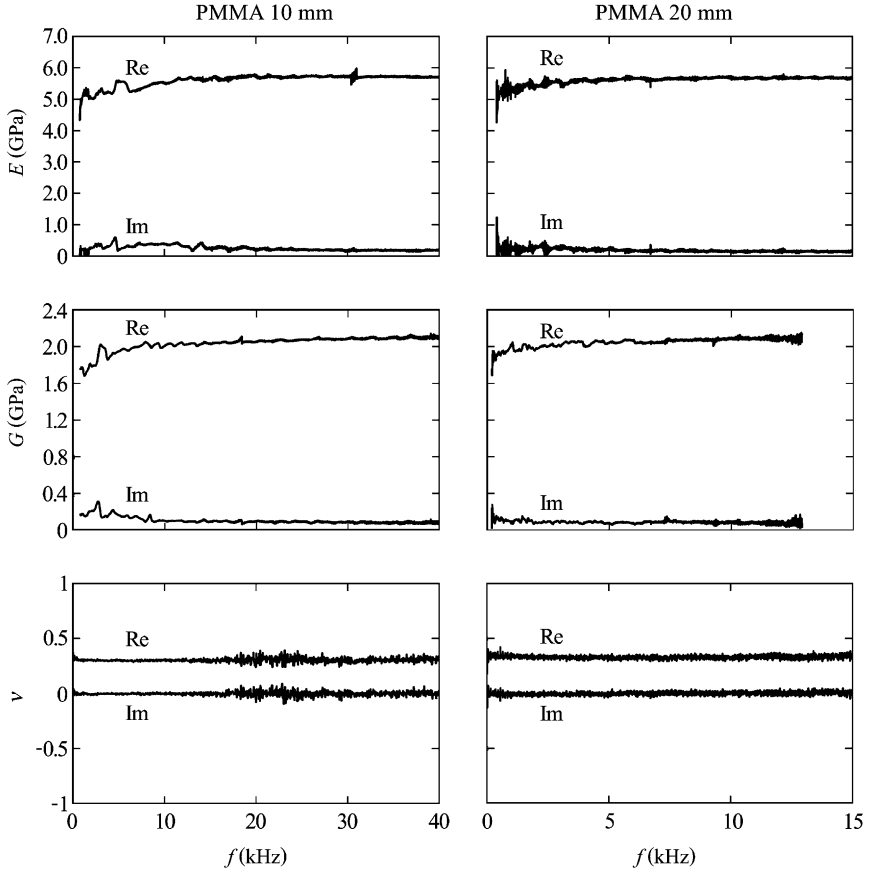

Fig. 5. Complex extension modulus E, complex shear modulus G and complex Poisson's ratio v of PMMA versus frequency f for 10 and 20 mm test bars.

maxima somewhere between 5°and 9° at low frequencies, and they decrease to about 2° at higher frequencies. For PP these loss angles are about 8–12° in the frequency range studied. This confirms that PP has higher losses than PMMA.

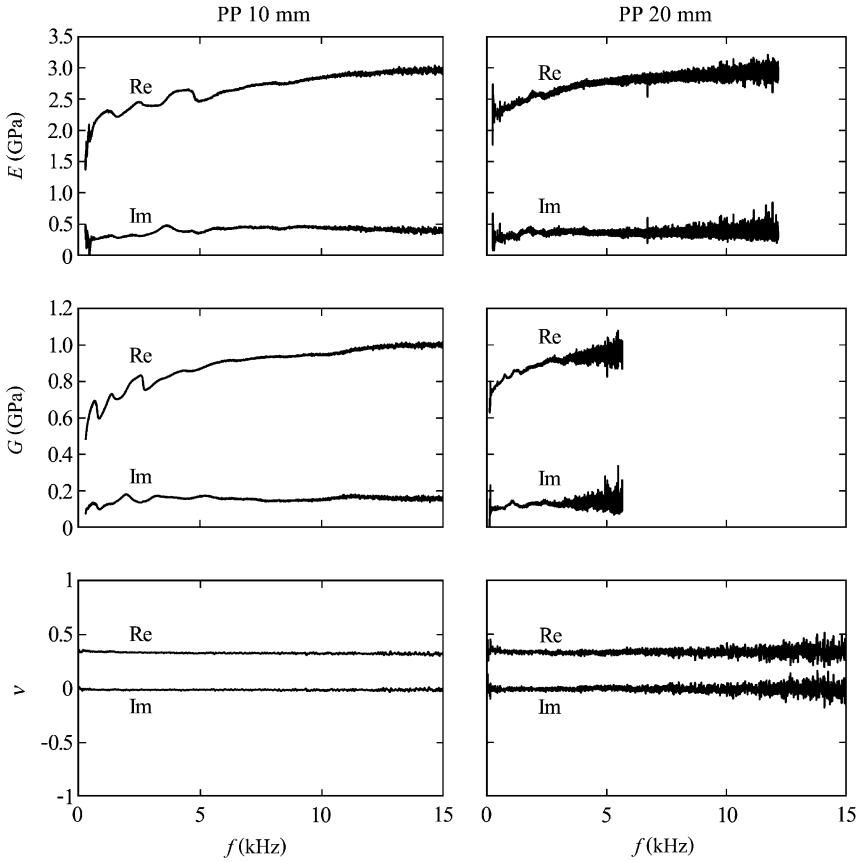

Fig. 6. Complex extension modulus E, complex shear modulus G and complex Poisson's ratio v of PP versus frequency f for 10 and 20 mm test bars.

Figs. 5 and 6 show that for the 20 mm test bars, the identification procedure for E and G suffered from convergence problems at higher frequencies, especially for PP. The reason is that it was more difficult to achieve sufficient excitation at high frequencies with the 20 mm test bars than with the 10 mm ones, and with PP than with PMMA due to the higher losses. In the case of G, the difficulty with the 20 mm test bars was largely due to the filtering effect of the aluminium ring clamped on the impacted bar end.

The ratios of the complex extension moduli E_{HI}/E_{LO} and of the complex shear moduli G_{HI}/G_{LO} at high (index HI) and low (index LO) levels of impact excitation are shown versus frequency f in Fig. 9 for PMMA and in Fig. 10 for PP. For both materials, these ratios are approximately real and equal to unity, which indicates that the responses are very close to linear under the conditions of the tests.

The ratio $2(1+v)G/E$ is shown versus frequency f in Fig. 11 for PMMA and in Fig. 12 for PP. For a material with isotropic response, this ratio is expected to be real and equal to unity. For PMMA with both test bars and for PP with the 20 mm test bar, this is approximately the case. For PP with the 10 mm test bar, the ratio is approximately real but somewhat smaller than unity

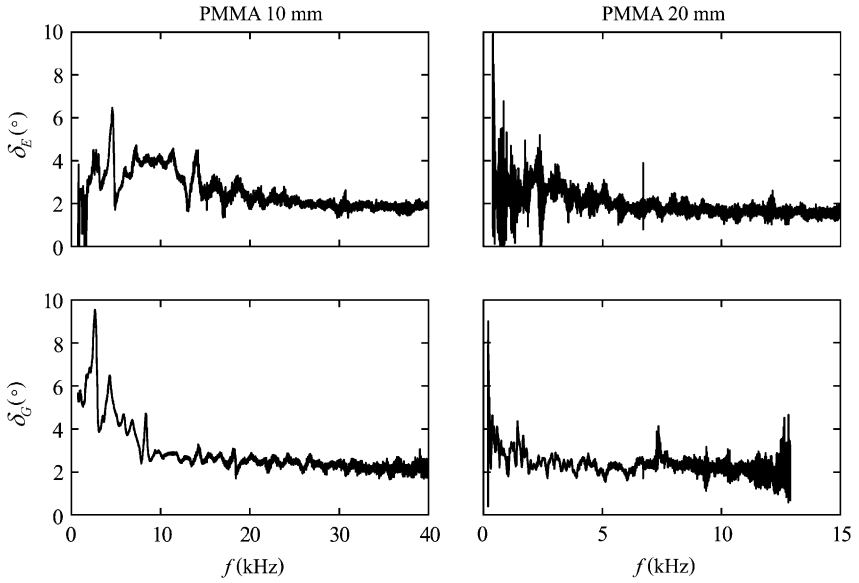

Fig. 7. Loss angles $\delta_E = \arg(E)$ and $\delta_G = \arg(G)$ of PMMA versus frequency f for 10 and 20 mm test bars.

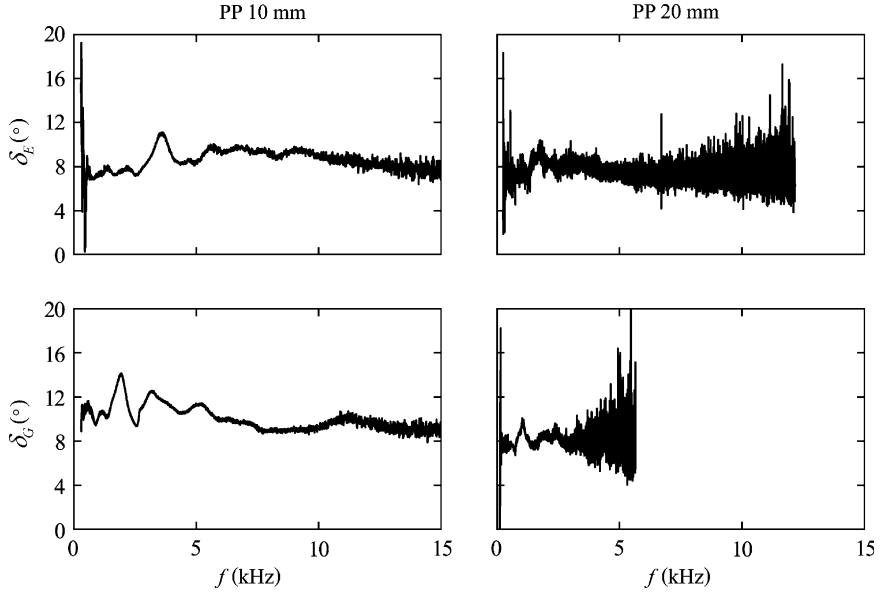

Fig. 8. Loss angles $\delta_E = \arg(E)$ and $\delta_G = \arg(G)$ of PP versus frequency f for 10 and 20 mm test bars.

($\approx$ 0.9), which indicates a certain degree of anisotropy. It is believed that some real anisotropy may be due to the extrusion process used for fabrication of the PP test bars. If this process affects the orientation of molecules within a certain depth under the surface, the influence on the 10 mm test bars can be expected to be larger than that on the 20 mm test bars. Some apparent anisotropy

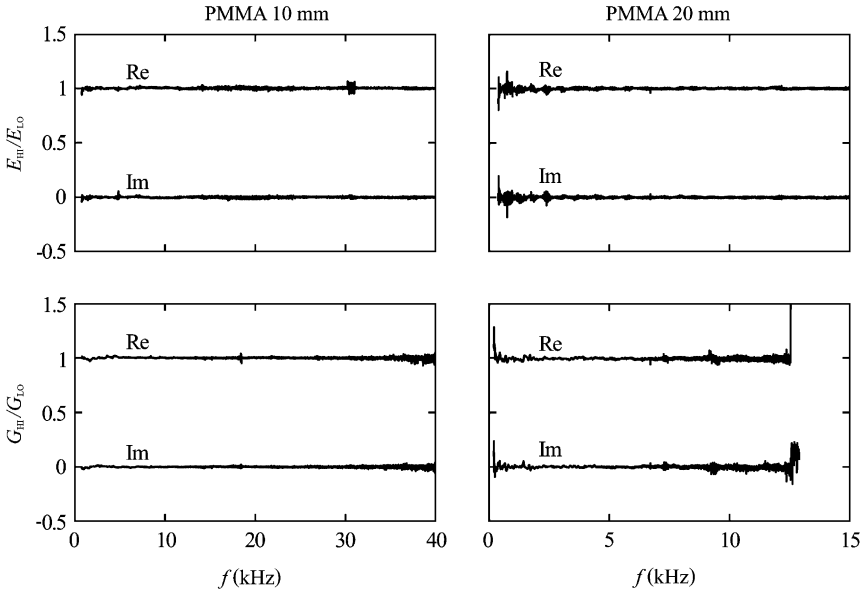

Fig. 9. Ratios of complex extension moduli E_{HI}/E_{LO} and complex shear moduli G_{HI}/G_{LO} of PMMA at high (HI) and low (LO) levels of impact excitation versus frequency f for 10 and 20 mm test bars.

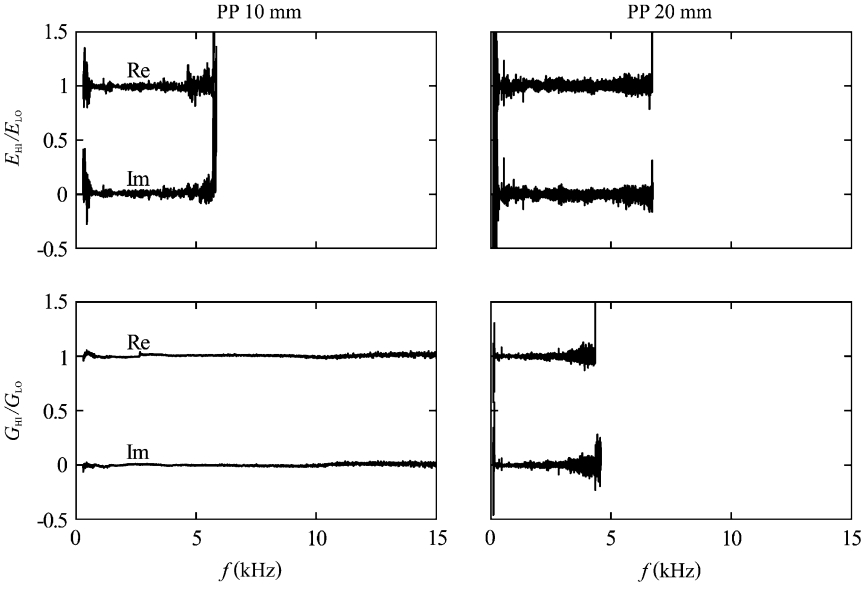

Fig. 10. Ratios of complex extension moduli E_{HI}/E_{LO} and complex shear moduli G_{HI}/G_{LO} of PP at high (HI) and low (LO) levels of impact excitation versus frequency f for 10 and 20 mm test bars.

may be due to the slight deviation from circular shape of the cross-sections of the PP test bars caused by the cooling process. This deviation can be expected to have a certain effect on the estimated value of G but not on that of E.

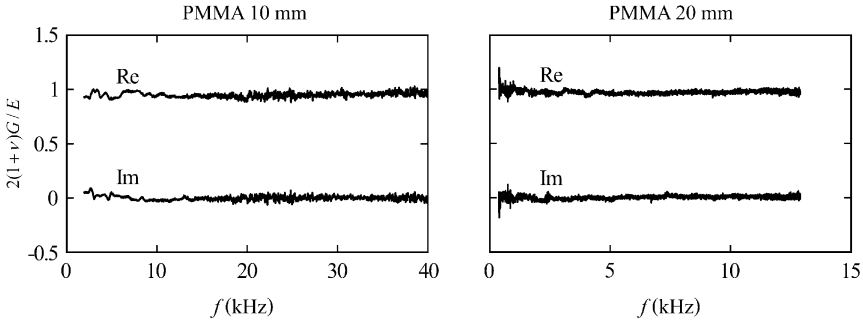

Fig. 11. Ratio $2(1+v)G/E$ of PMMA versus frequency f for 10 and 20 mm test bars.

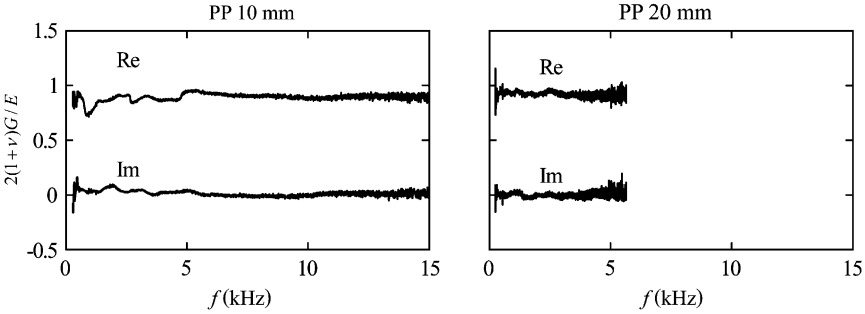

Fig. 12. Ratio $2(1+v)G/E$ of PP versus frequency f for 10 and 20 mm test bars.

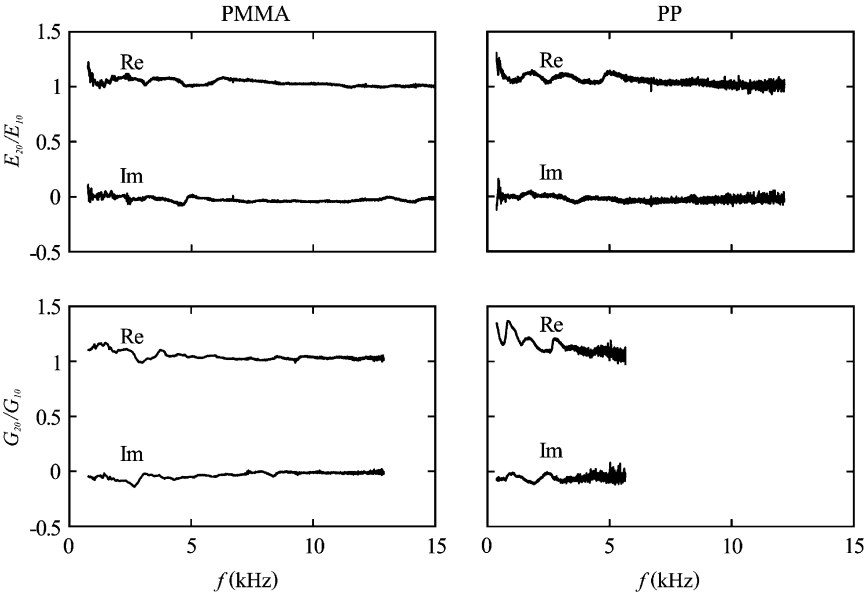

Fig. 13. Ratios of complex extension moduli E_{20}/E_{10} and complex shear moduli G_{20}/G_{10} of PMMA and PP versus frequency f for 10 and 20 mm test bars.

The ratios of complex extension moduli E_{20}/E_{10} and of complex shear moduli G_{20}/G_{10} are shown versus frequency f for PMMA and PP in Fig. 13, where indices 10 and 20 refer to the diameters in mm of the test bars. If the results of the identification procedures do not depend on the test bars, and the mechanical properties of each material are the same for the 10 and 20 mm test bars, these ratios are expected to be real and equal to unity. For PMMA this is approximately the case for both ratios of complex moduli except at low frequencies, where there is a certain deviation. For PP the deviation from unity is larger, especially at low frequencies. It is believed that this larger deviation for PP may be partly due to the different effects of the extrusion process on the 10 and 20 mm test bars.

5. Conclusions

The complex extension modulus, the complex shear modulus and the complex Poisson's ratio at room temperature have been identified for polymethyl methacrylate (PMMA) and polypropylene (PP) in the approximate frequency range 1–40 kHz for PMMA and 1–15 kHz for PP. The responses of both materials were found to be very close to linear and nearly isotropic under the conditions of the tests. The deviation from isotropy was larger for PP than that for PMMA, especially for the 10 mm test bars. A certain influence of the test bar dimension on the complex moduli was observed, especially for PP at low frequencies. The influence of test bar dimension on the observed deviation from isotropy and on the complex moduli for PP is believed to be partly due to the extrusion and cooling processes used for fabrication of the PP test bars.

Acknowledgements

The authors wish to thank Dr. Lars Hillström for provision of identification software and helpful discussions. Funding from the Swedish Research Council for Engineering Sciences (TFR) under contract 2000-587 is gratefully acknowledged.

Appendix A. Nomenclature

a radius of cross-section
$\mathbf{A}$ matrix ($n \times 2$)
E complex extension modulus
$\tilde{e}$ error
f frequency ($= \omega/2\pi$)
G complex shear modulus
k wavenumber ($= 2\pi/\lambda$)
M complex modulus ($= E$ or G)
n number of equations or elements
$\hat{N}$ complex amplitude of harmonic wave
$\hat{P}$ complex amplitude of harmonic wave

r radial co-ordinate
t time
$\hat{\mathbf{w}}$ amplitude vector (2×1; elements $\hat{P}$, $\hat{N}$)
z axial co-ordinate
α damping coefficient
γ wave propagation coefficient ($= \alpha + \mathrm{i}k$)
δ loss angle
ε strain (extension or shear)
$\hat{\boldsymbol{\varepsilon}}$ strain vector ($n \times 1$; elements $\hat{\varepsilon}_1, \hat{\varepsilon}_2, \ldots, \hat{\varepsilon}_n$)
λ wavelength ($= 2\pi/k$)
ν complex Poisson's ratio
ρ density
φ angular co-ordinate
ω angular frequency ($= 2\pi f$)

References

[1] P.S. Theocaris, Interrelation between dynamic moduli and compliances in polymers, *Kolloid-Zeitschrift und Zeitschrift für Polymere* 235 (1960) 1182–1188.
[2] T. Pritz, Frequency dependences of complex moduli and complex Poisson's ratio of real solid materials, *Journal of Sound and Vibration* 214 (1998) 83–104.
[3] H. Kolsky, S.S. Lee, The propagation and reflection of stress pulses in linear viscoelastic media, Technical Report No. 5, Brown University Providence, RI, 1962.
[4] P.S. Theocaris, N. Papadopoulou, Propagation of stress waves in viscoelastic media, *Polymer* 19 (1978) 215–219.
[5] R.H. Blanc, Détermination de l'Équation de Comportement des Corps Viscoélastiques Linéaires par une Méthode d'Impulsion, Ph.D. Thesis, Université d'Aix-Marseille, 1971, Published in part in: W.K. Nowacki (Ed.), Problèmes de la Rhéologie, 65-85, IPPT PAN, Warsaw 1973.
[6] R.H. Blanc, Progress in pulse testing methods for viscoelastic solids, *Proceedings of the Second National Congress on Theoretical and Applied Mechanics*, Vol. 2, Varna, Bulgarian Academy of Science Publication, Sofia, 1976, pp. 555–564.
[7] R.H. Blanc, Transient wave propagation methods for determining the viscoelastic properties of solids, *Journal of Applied Mechanics* 60 (1993) 763–768.
[8] Y. Sogabe, K. Kishida, K. Nakagawa, Wave propagation analysis for determining the dynamic properties of high damping alloys, *Bulletin of the Japan Society of Mechanical Engineers* 25 (1982) 321–327.
[9] Y. Sogabe, M. Tsuzuki, Identification of the dynamic properties of linear viscoelastic materials by the wave propagation testing, *Bulletin of the Japan Society of Mechanical Engineers* 29 (1986) 2410–2417.
[10] J.L. Buchanan, Numerical solution for the dynamic moduli of a viscoelastic bar, *Journal of the Acoustical Society of America* 81 (1987) 1775–1786.
[11] B. Lundberg, R.H. Blanc, Determination of mechanical material properties from the two-point response of an impacted linearly viscoelastic rod specimen, *Journal of Sound and Vibration* 126 (1988) 97–108.
[12] S. Ödeen, B. Lundberg, Determination of complex modulus from measured end-point accelerations of an impacted rod specimen, *Journal of Sound and Vibration* 165 (1993) 1–8.
[13] B. Lundberg, S. Ödeen, In situ determination of the complex modulus from strain measurements on an impacted structure, *Journal of Sound and Vibration* 167 (1993) 413–419.
[14] A.J. Hull, An inverse method to measure the axial modulus of composite materials under tension, *Journal of Sound and Vibration* 195 (1996) 545–551.
[15] M. Soula, T. Vinh, Y. Chevalier, T. Beda, C. Esteoule, Measurements of isothermal complex moduli of viscoelastic materials over a large range of frequencies, *Journal of Sound and Vibration* 205 (1997) 167–184.

[16] L. Hillström, M. Mossberg, B. Lundberg, Identification of complex modulus from measured strains on an axially impacted bar using least squares, *Journal of Sound and Vibration* 230 (2000) 689–707.
[17] L. Hillström, U. Valdek, B. Lundberg, Estimation of the state vector and identification of the complex modulus of a beam, *Journal of Sound and Vibration* 261 (2003) 653–673.
[18] M. Mossberg, L. Hillström, L. Abrahamsson, Parametric identification of viscoelastic materials from time and frequency domain data, *Inverse Problems in Engineering* 9 (2001) 645–670.
[19] I. Kennedy, G.R. Tomlinson, Torsional vibration transmissibility characteristics of reinforced viscoelastic flexible pipes, *Journal of Sound and Vibration* 122 (1988) 149–169.
[20] T. Pritz, Measurement methods of complex Poisson's ratio of viscoelastic materials, *Applied Acoustics* 60 (2000) 279–292.
[21] S.C. Hunter, Viscoelastic waves, in: I.N. Sneddon, R. Hill (Eds.), *Progress in Solid Mechanics*, Vol. 1, North-Holland, Amsterdam, 1960, pp. 3–56.